Experimental investigation and modeling of the fine structure splitting of neutral excitons in strain-free GaAs/Al$_x$Ga$_{1-x}$As quantum dots

J. D. Plumhof,[1] V. Křápek,[1,2] L. Wang,[1,3] A. Schliwa,[4] D. Bimberg,[4] A. Rastelli,[1,*] and O. G. Schmidt[1]

[1]*Institute for Integrative Nanosciences, IFW Dresden, Helmholtzstr. 20, D-01069 Dresden, Germany*
[2]*Institute of Condensed Matter Physics, Masaryk University, Kotlářská 2, 61137 Brno, Czech Republic*
[3]*Max Planck Institute for Solid State Research, Heisenbergstr. 1, D-70569 Stuttgart, Germany*
[4]*Institut für Festkörperphysik, Technische Universität Berlin, Hardenbergstr. 36, D-10623 Berlin, Germany*

We measure, by photoluminescence spectroscopy, the fine structure splitting (FSS) of bright excitons confined in a large number of elongated and unstrained Al$_{0.35}$Ga$_{0.65}$As/GaAs/Al$_{0.45}$Ga$_{0.55}$As quantum dots (QDs) and quantum-well potential fluctuations (QWPFs). While the FSS values are comparable, the light polarization directions for well-oriented QDs and randomly oriented QWPFs on the same sample are substantially different. We compare the results with model calculations using as input scanning probe microscopy data of QD structures nominally identical to those investigated by photoluminescence. The model reproduces well the polarization orientation for all studied samples and also the magnitude of the FSS, at least for relatively tall dots. We discuss the results and elucidate the role of in-plane elongation on the FSS.

PACS number(s): 78.67.Hc, 81.07.Ta

Semiconductor quantum dots (QDs) keep attracting much interest due to their potential applications in the field of quantum information processing and communication. As an example, the biexciton-exciton radiative cascade in QDs can be used to generate entangled photon pairs.[1] The neutral exciton consists of two optically dark and two bright states. The energies of the bright states are usually separated by an energy of several tens of micro-electronvolts. This separation, known as fine structure splitting (FSS),[2] is attributed to the anisotropic electron-hole exchange interaction.[3,4] The FSS destroys the polarization entanglement of photons, which can be achieved only on rare QDs with FSS on the order of the homogeneous linewidth[5,6] or by using spectral filtering.[7] For this reason, the FSS of excitons in QDs is currently an active field of research with the aim of better understanding its origin[8–10] and predicting strategies to reduce it.[11]

Despite the efforts, a direct and quantitative comparison of theoretical with experimental results on FSS of QDs remains difficult. This is mostly due to the lack of accurate structural parameters taken into the model, which often results in inconsistencies between theory and experiment. In fact, most of the previous investigations on FSS focused either on strained and intermixed Stranski-Krastanow (SK) QDs (Refs. 12 and 13) where the alloy composition profiles are difficult to access or on potential fluctuations in thin quantum wells (QWs), which have poorly defined shape.[2,14,15] Besides that, the theoretical predictions depend strongly on the employed models,[8] which should be tested on QDs with well-known structural parameters. Therefore, theory and experiments on FSS have remained so far relatively disjointed. Unstrained GaAs/AlGaAs QDs with good structural homogeneity[16–18] are ideally suited to address this problem. Only very recently, Abbarchi *et al.*[19,20] studied the FSS of GaAs QDs but the correlation between FSS and QD morphology was kept at a qualitative level.

In this work, we measure the FSS of "hierarchically self-assembled" GaAs/AlGaAs QDs (Ref. 17) and make a direct comparison with calculations based on eight-band $k \cdot p$ and the configuration-interaction models. We determine the optical properties (FSS and polarization orientation) and the morphology of hundreds of QDs. Due to the lack of lattice mismatch and choice of growth conditions, intermixing, strain, and piezoelectricity are negligible in our QD system. We therefore use the experimentally determined shapes and nominal growth parameters as input for the calculations. We find that the model reproduces well the polarization orientation for all studied samples and also the magnitude of the FSS, at least for relatively tall dots. The agreement on the FSS values is somewhat poorer for flatter dots, where the model predicts values which are generally larger than the observed ones. The comparison between the polarization directions for QDs and for QW potential fluctuations (QWPFs) allows us to highlight the dominant contribution of the shape asymmetry in determining the FSS for the investigated system.

The studied QDs were grown by molecular-beam epitaxy combined with *in situ* selective etching. The latter is used to create nanoholes (NHs) on the GaAs surface starting from SK InAs/GaAs islands.[21] The NHs are overgrown with an Al$_{0.45}$Ga$_{0.55}$As layer of thickness D serving as bottom barrier at a nominal substrate temperature of 500 °C. During AlGaAs overgrowth, the shape of the NHs changes slightly, their depth decreases, while their elongation along the [110] axis is maintained.[17] After AlGaAs growth, the NHs are filled by depositing nominal 2 nm of GaAs followed by a 2 min growth interruption, which allows the diffusion of GaAs into the NHs. The deposition of a top Al$_{0.35}$Ga$_{0.65}$As barrier yields inverted unstrained GaAs QDs surrounded by a thin GaAs QW. The obtained QDs are characterized by a good size homogeneity resulting in photoluminescence (PL) ensemble linewidths down to ~10 meV, which allows the comparison with theoretical simulations. By terminating the growth right after the deposition of the Al$_{0.45}$Ga$_{0.55}$As bottom barrier, we determined the shape of the AlGaAs NHs and hence of the GaAs QDs using scanning tunneling microscopy or atomic force microscopy (STM/AFM). We used AFM to collect data with large statistics and ultrahigh-
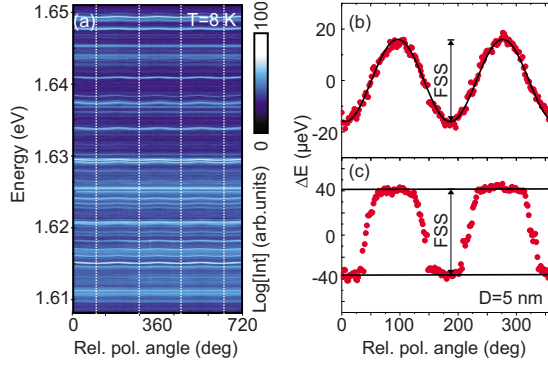
FIG. 1. (Color online) (a) Color-coded PL intensity recorded for varying polarization angle from the sample with $D=5$ nm. The white lines indicate the angles corresponding to emission polarization along the [110] crystal direction. (b) and (c) Results of Lorentzian fits of two split excitonic lines with relatively (b) small and (c) large FSS. The FSS is obtained from the amplitude of a sine fit in (b) or from the energy separation between the top and bottom flat regions in (c). See text for details.

vacuum STM to image the roughness of the AlGaAs layer. Three NH samples with $D=5$, 7, and 10 nm were investigated with AFM and three QD samples produced with the same nominal growth parameters were studied by PL spectroscopy.

The optical investigations were carried out in a standard micro-PL setup at 8 K, with a spectral resolution of ~ 70 μeV. The linear polarization of the QD emission was measured by continuous rotation of a $\lambda/2$ wave plate followed by a linear polarizer in front of the spectrometer. By using samples with relatively high QD density (some 10^9 cm^{-2}), we investigated up to 15 QDs within one measurement cycle, similar to the approach of Ref. 12.

Figure 1(a) shows an example of the PL intensity as the $\lambda/2$ wave plate is rotated by 360° (corresponding to 720° of polarization angle). The laser power was set well below saturation to keep biexciton emission below the detection limit. Each spectrum consists of a number of sharp recombination lines originating from different dots. The wavy patterns are ascribed to the FSS of neutral excitons (both fine structure splitted photons have orthogonal linear polarization). Several lines showing no FSS are attributed to positive trions.[22] All neutral exciton lines appear to "oscillate" in phase in Fig. 1(a), indicating a rather homogeneous orientation of the low- and high-energy components of the doublets.

For the determination of the FSS, we first fit the different excitonic lines with Lorentzian curves as a function of the polarization angle. The results for two representative QDs are shown in Figs. 1(b) and 1(c). Depending on the amplitude of the FSS, the obtained peak positions follow a pattern resembling either a sine wave [for relatively small FSS, where the two components are not spectrally resolved, see Fig. 1(b)] or a square wave [for larger FSS, where the two components are spectrally resolved even without polarization selection, see Fig. 1(c)]. In both cases, we then fit the wavy pattern with a sine function to determine the polarization orientation of the low-energy component of the doublet relative to the [110] crystal direction. In the former case, the sine fit provides also a reliable measure of the FSS [Fig. 1(b)]

while in the latter case, we obtain the FSS by fitting the flat regions of the "square wave" with two constant functions and measuring the energy difference [Fig. 1(c)]. The uncertainty of the FSS is estimated to be $\sim (^{+10}_{-5})$ μeV.

Our theoretical simulation of the FSS consists of two steps. First, single-particle states are calculated by eight-band $k \cdot p$ theory by using the structural information obtained by AFM and nominal growth parameters. The shape of the QDs is discretized in steps of 0.5 nm. (A test with 0.25 nm resolution yielded to comparable results.) The resulting wave functions are expressed as

$$\psi_i(\vec{r}) = \sum_{n=1}^{8} \chi_{i,n}(\vec{r}) u_n(\vec{r}),$$

where i is an index of the wave function, $\chi_{i,n}(\vec{r})$ are the so-called envelope functions, and $u_n(\vec{r})$ are Bloch waves in the Γ point. The summation goes over six valence and two conduction bands. Details are given elsewhere.[10,23]

The second step is the configuration-interaction calculation of the exciton states. The exciton wave function $|X\rangle$ is expanded into the basis of configurations $|C(c\alpha, v\beta)\rangle$,

$$|X\rangle = \sum_{\alpha, \beta} |C(c\alpha, v\beta)\rangle, \quad |C(c\alpha, v\beta)\rangle = \hat{a}_{c\alpha}^+ \hat{a}_{v\beta} |0\rangle.$$

Here α (β) is the index of conduction (valence) single-particle state (the auxiliary labels c and v help to distinguish between conduction and valence electrons), $\hat{a}_i^+$ and $\hat{a}_i$ are the creation and annihilation operators of the ith single-particle state, and $|0\rangle$ is the "vacuum" state (i.e., the valence-electron states are occupied and conduction-electron states are empty).

The exciton Hamiltonian matrix elements are

$$\langle C(c\alpha, v\beta)|\hat{H}|C(c\gamma, v\delta)\rangle$$
$$= (E_{c\alpha} - E_{v\beta})\delta_{\alpha\gamma}\delta_{\beta\delta} - V_{c\alpha \ v\delta, c\gamma \ v\beta} + V_{c\alpha \ v\delta, v\beta \ c\gamma}$$

with

$$V_{ij,kl} = \int \int d^3\vec{r}_1 d^3\vec{r}_2 \frac{\psi_i^*(\vec{r}_1)\psi_j^*(\vec{r}_2)e^2 \psi_k(\vec{r}_1)\psi_l(\vec{r}_2)}{4\pi\varepsilon_0\varepsilon_r|\vec{r}_1 - \vec{r}_2|}.$$

Here E_i are single-particle energies, e is the elementary charge, ε_0 is the vacuum permittivity, and ε_r is the dielectric constant. The terms $-V_{c\alpha \ v\delta, c\gamma \ v\beta}$ and $V_{c\alpha \ v\delta, v\beta \ c\gamma}$ represent direct and exchange Coulomb interaction, respectively.

The evaluation of Coulomb matrix elements was carried out following mostly the procedure of Takagahara.[9] The important extension is that we included more terms (zeroth and first order) in the expansion 2.9 of Ref. 9, which were zero in previous works[8,9] because of neglected mixing between conduction and valence bands in single-particle calculations. The energies of the exciton states are found by the Hamiltonian diagonalization and the FSS is retrieved as the energy difference between the two lowest bright exciton states.

The left insets in Fig. 2 show images of NHs on samples with different D obtained by numerical averaging of AFM topographs of around 50 AlGaAs NHs. The average depth of the NHs is 4.8 ± 0.4, 4.1 ± 0.3, and 3.3 ± 0.4 nm for $D=5$, 7, and 10 nm, respectively. While most of the NHs on the same
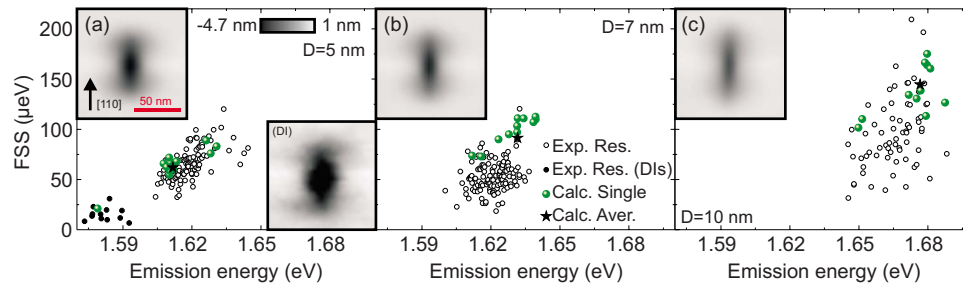
FIG. 2. (Color online) Experimental (black circles) and calculated (dots and stars) FSS as a function of exciton energy for samples with (a) $D=5$, (b) 7, and (c) 10 nm. The filled black circles in (a) correspond to QDs created from DIs. The black stars are the FSS calculated for the averaged depth profiles (insets in the upper left corners of each panel). The inset in the lower right corner in (a) shows the depth profile of a NH created by etching of a DI. The scale of all insets is specified in (a).

sample have rather homogeneous size and orientation, as they are produced by etching of coherent InAs islands with a good size homogeneity, some deeper (about 7 nm) NHs are found in the sample with $D=5$ nm [right inset in Fig. 2(a)]. These nanostructures are likely to originate from relatively large dislocated InAs islands (DIs). Figure 2 shows the relation between FSS and emission energy for QDs in the three different samples. Besides the experimental data (circles), we show the results of the calculations for ten different NHs, which were randomly chosen in the AFM images of each sample (dots) as well as for the averaged shapes (stars). In all plots, we see that the calculation results (dots) corresponding to GaAs dots obtained by etching of coherent InAs islands display "bimodal" distributions in the emission energy (i.e., an apparent gap located, e.g., around 1.62 eV for the sample with $D=5$ nm). This is due to the discretization step size of 0.5 nm used in the calculations.

We first focus on the sample with $D=5$ nm [Fig. 2(a)]. The experimental exciton energy displays a bimodal distribution. QDs emitting at low energy have small FSS (down to ~ 10 μeV) while QDs emitting at higher energy have larger FSS (~ 66 μeV). We ascribe the low-energy emission lines to excitons confined in QDs obtained by etching of DIs. (The fact that these QDs are optically active is interesting, as it indicates that the InAs material and crystal defects are removed during the AsBr$_3$ etching step leaving behind deeper NHs, which can be used as a template to create defect-free GaAs/AlGaAs QDs.) In spite of the spread in FSS values for both families of dots, we also see that the FSS tends to increase with increasing emission energy. The points corresponding to the calculation results for both QD families are well overlapped with the experimental data, indicating that the used model is able to reproduce the emission energies, the magnitude of the FSS, and also the trend of increasing FSS with energy.

If we now compare the images of the NHs in the top insets of Fig. 2, we see that dots tend to become more elongated with increasing D.[17] Qualitatively, we would thus expect an increase in FSS, as also confirmed by the calculations [compare the stars in Figs. 2(a)–2(c)]. The experimental results do not follow however such a clear trend. For the samples with $D=5$, 7, and 10 nm, the average values of the FSS change from 66, to 53 to 96 μeV, with standard deviations increasing with D from 23 to 28 and to 38%, respectively. The broadening of the distributions of the FSS with

increasing D can be partly ascribed to the broadening of the distribution of size and shapes of the NHs, which become more irregular as D increases.[17] For the samples with $D=7$ and 10 nm, the calculated and experimental points show some overlap but the predicted FSS values are generally larger and their distribution more homogeneous than the observed ones. Although we cannot definitely track the origin of the poorer agreement compared to the sample with $D=5$ nm, we note that for increasing D, the NH depth decreases so that monolayer-high asperities of the bottom or top AlGaAs interfaces (which are below the resolution used in the calculation) may lead to exciton confinement in a small region of the QD, similar to QW thickness fluctuations. Furthermore, as the dots become flatter, the spilling of the exciton wave function in the alloy barrier increases: alloy disorder (an atomistic effect which is not treated in our model) may contribute to the broadening of the FSS distributions.[24]

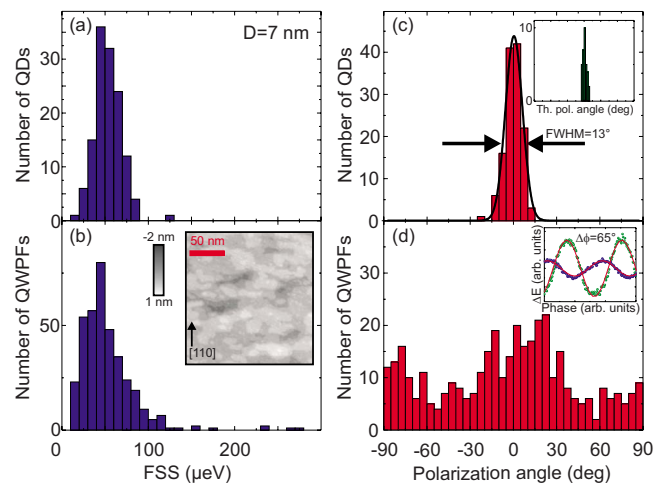To obtain an idea about the contribution of effects other

FIG. 3. (Color online) (a) Histogram of the FSS values for QDs and (b) QWPFs measured on the sample with $D=7$ nm. (c) Polarization direction of the low-energy component of the exciton for the QDs and (d) for the QWPFs. A polarization angle of 0° corresponds to the [110] crystal direction. The inset in (b) shows an STM image of the lower barrier of the QW. The inset in (c) shows the calculated polarization distribution for NHs with $D=5$, 7, and 10 nm; the x-axis scale is the same as for the main axis panel. The inset in (d) shows the polarization behavior of two representative QWPF emission lines with relative polarization angle $\Delta\phi$.

than shape anisotropy[24] (e.g., crystal anisotropy, alloy disorder, etc.) to the FSS of our QDs, we studied experimentally the FSS of excitons confined in the potential fluctuations of the rough QW between the QDs. The distribution of the FSS values for the QDs [Fig. 3(a)] in the sample with $D = 7$ nm is slightly narrower compared to the distribution for the QW-PFs [Fig. 3(b)] of the same sample but the average values are comparable. On the other hand, the polarization direction of light emitted by excitons confined in QDs and QWPFs is remarkably different [Figs. 3(c) and 3(d)]. The low-energy component of the bright excitons in QDs shows a pronounced alignment along the [110] crystal direction [Fig. 3(c)], in all investigated samples. We attribute this finding to the homogeneity in elongation of the AlGaAs NHs. A detailed analysis of around 400 NHs shows in fact that the NHs for all values of D are aligned within $\pm 7°$ with respect to the [110] crystal axis (not shown). This polarization distribution is also reproduced by our simulations on QDs with $D = 5$, 7, and 10 nm [inset of Fig. 3(c)] and it appears different from previous studies[3,20] where the high-energy component of the doublets was observed to be parallel to the long QD axis. The reason for this discrepancy is at present unclear. The polarization of light emitted by QWPFs is rather randomly oriented [see Fig. 3(d) and inset], with only a slight preferential alignment along the [110] and [1$\bar{1}$0] directions. We mainly ascribe this observation to the irregular shape of the confining potentials created by the bottom QW barrier [see STM image in the inset of Fig. 3(b)]. (We expect the top QW interface to be smoother because of the larger diffusivity of Ga compared to Al and the annealing step following GaAs growth.)

Finally, we have also measured the polarization direction for QDs obtained by filling AlGaAs NHs ($D = 10$ nm) with only 0.5 nm GaAs. In this case, the emission energies are very close to those of the QWPFs but the polarization of the exciton emission is very similar to that observed for the taller dots discussed here: the low-energy component of the exciton is invariably polarized along directions close to the [110].

In conclusion, we have studied experimentally and theoretically the fine structure splitting of neutral excitons in elongated and unstrained GaAs QDs embedded in AlGaAs barriers. The calculations, which are based on the measured structure and nominal growth parameters, are able to reproduce well the polarization orientation for all studied dots and also the magnitude of the splitting for relatively tall dots. For flatter dots, the predicted values are however slightly larger than the observed ones. Finally, we highlight the impact of shape anisotropy on the FSS by comparing measurements on QDs and on randomly oriented QW potential fluctuations on the same samples.

*a.rastelli@ifw-dresden.de

[1] O. Benson, C. Santori, M. Pelton, and Y. Yamamoto, Phys. Rev. Lett. **84**, 2513 (2000).

[2] D. Gammon, E. S. Snow, B. V. Shanabrook, D. S. Katzer, and D. Park, Phys. Rev. Lett. **76**, 3005 (1996).

[3] L. Besombes, K. Kheng, and D. Martrou, Phys. Rev. Lett. **85**, 425 (2000).

[4] M. Bayer *et al.*, Phys. Rev. B **65**, 195315 (2002).

[5] R. Hafenbrak, S. M. Ulrich, P. Michler, L. Wang, A. Rastelli, and O. G. Schmidt, New J. Phys. **9**, 315 (2007).

[6] R. Stevenson, R. Young, P. Atkinson, K. Cooper, D. Ritchie, and A. Shields, Nature (London) **439**, 179 (2006).

[7] N. Akopian, N. H. Lindner, E. Poem, Y. Berlatzky, J. Avron, D. Gershoni, B. D. Gerardot, and P. M. Petroff, Phys. Rev. Lett. **96**, 130501 (2006).

[8] E. Poem, J. Shemesh, I. Marderfeld, D. Galushko, N. Akopian, D. Gershoni, B. D. Gerardot, A. Badolato, and P. M. Petroff, Phys. Rev. B **76**, 235304 (2007).

[9] T. Takagahara, Phys. Rev. B **62**, 16840 (2000).

[10] O. Stier, M. Grundmann, and D. Bimberg, Phys. Rev. B **59**, 5688 (1999).

[11] R. Singh and G. Bester, Phys. Rev. Lett. **103**, 063601 (2009).

[12] S. Seidl, B. Gerardot, P. Dalgarno, K. Kowalik, A. Holleitner, P. Petroff, K. Karrai, and R. Warburton, Physica E **40**, 2153 (2008).

[13] R. Seguin, A. Schliwa, S. Rodt, K. Pötschke, U. W. Pohl, and D. Bimberg, Phys. Rev. Lett. **95**, 257402 (2005).

[14] C. Ropers *et al.*, Phys. Rev. B **75**, 115317 (2007).

[15] M. Ramsteiner, R. Hey, R. Klann, U. Jahn, I. Gorbunova, and K. H. Ploog, Phys. Rev. B **55**, 5239 (1997).

[16] C. Heyn, A. Stemmann, T. Koppen, C. Strelow, T. Kipp, M. Grave, S. Mendach, and W. Hansen, Appl. Phys. Lett. **94**, 183113 (2009).

[17] A. Rastelli, S. Stufler, A. Schliwa, R. Songmuang, C. Manzano, G. Costantini, K. Kern, A. Zrenner, D. Bimberg, and O. G. Schmidt, Phys. Rev. Lett. **92**, 166104 (2004).

[18] K. Leifer, E. Pelucchi, S. Watanabe, F. Michelini, B. Dwir, and E. Kapon, Appl. Phys. Lett. **91**, 081106 (2007).

[19] M. Abbarchi, T. Kuroda, C. Mastrandrea, A. Vinattieri, S. Sanguinetti, T. Mano, K. Sakoda, and M. Gurioli, Physica E **42**, 881 (2010).

[20] M. Abbarchi, C. A. Mastrandrea, T. Kuroda, T. Mano, K. Sakoda, N. Koguchi, S. Sanguinetti, A. Vinattieri, and M. Gurioli, Phys. Rev. B **78**, 125321 (2008).

[21] R. Songmuang, S. Kiravittaya, and O. G. Schmidt, Appl. Phys. Lett. **82**, 2892 (2003).

[22] L. Wang, V. Křápek, F. Ding, F. Horton, A. Schliwa, D. Bimberg, A. Rastelli, and O. G. Schmidt, Phys. Rev. B **80**, 085309 (2009).

[23] V. Mlinar, A. Schliwa, D. Bimberg, and F. M. Peeters, Phys. Rev. B **75**, 205308 (2007).

[24] V. Mlinar and A. Zunger, Phys. Rev. B **79**, 115416 (2009).